

Optical Bound States in the Continuum with Nanowire Geometric Superlattices

Seokhyoung Kim,¹ Kyoung-Ho Kim,^{1,2,*} and James F. Cahoon^{1,†}

¹*Department of Chemistry, University of North Carolina at Chapel Hill, Chapel Hill, North Carolina 27599-3290, USA*

²*Department of Physics, Chungbuk National University, Cheongju 28644, Republic of Korea*

 (Received 1 October 2018; published 10 May 2019)

Perfect trapping of light in a subwavelength cavity is a key goal in nanophotonics. Perfect trapping has been realized with optical bound states in the continuum (BIC) in waveguide arrays and photonic crystals; yet the formal requirement of infinite periodicity has limited the experimental realization to structures with macroscopic planar dimensions. We characterize BICs in a silicon nanowire (NW) geometric superlattice (GSL) that exhibits one-dimensional periodicity in a compact cylindrical geometry with a subwavelength diameter. We analyze the scattering behavior of NW GSLs by formulating temporal coupled mode theory to include Lorenz-Mie scattering, and we show that GSL-based BICs can trap electromagnetic energy for an infinite lifetime and exist over a broad range of geometric parameters. Using synthesized NW GSLs tens of microns in length and with variable pitch, we demonstrate the progressive spectral shift and disappearance of Fano resonances in experimental single-NW extinction spectra as a manifestation of BIC GSL modes.

DOI: [10.1103/PhysRevLett.122.187402](https://doi.org/10.1103/PhysRevLett.122.187402)

Trapping light in subwavelength structures is of utmost importance in wave physics [1–3] and is central to a wide range of photonic and optoelectronic applications [4–7]. Localized optical modes with infinite lifetimes—namely, optical bound states in the continuum (BICs)—can exist in the radiation continuum, and they have been described in one-dimensional (1D) arrays of coupled waveguides [8–10] and two-dimensional (2D) photonic crystals (PCs) [3,11,12]. Despite the subwavelength size of each optical resonator unit cell, however, BIC structures require infinite periodicity to formally satisfy the BIC condition [3], necessitating macroscopic quasi-infinite planar structures for experimental realization of both the 1D array and 2D PC examples. To reduce the physical dimensions of BIC cavities, recent theoretical studies have investigated the presence of BICs in 1D structures with lateral 2D confinement, such as 1D arrays of dielectric spheres [13,14] or disks [15,16], as well as supercavity modes in individual dielectric nanorods [17,18]. Optical BICs in these theoretical examples are reported to exist because of symmetry mismatch, accidental decoupling [13,15], or topological protection [14]. Although a detuned quasi BIC has been observed in the microwave regime from a chain of millimeter-sized ceramics [19], experimental demonstration of BICs in the optical regime with laterally confined 1D nanostructures has, to our knowledge, not been reported.

In this Letter, we describe the perfect trapping of light in single Si nanowire (NW) geometric superlattices (GSLs) through BICs above the light cone. A NW GSL has a subwavelength diameter that is periodically modulated along the NW axis [20–22], as shown in Fig. 1(a). The optical confinement defined by the NW diameter gives rise to well-defined, strong Mie resonances [23–25], allowing

NWs to strongly interact with external plane waves. Moreover, a NW GSL exhibits an additional set of unique photonic modes that are dependent on the pitch (p), outer diameter (d), and inner diameter (e) of the GSL. As shown herein, in a NW GSL under transverse-electric (TE) polarized plane wave illumination, GSL guided resonances [26] with different orbital angular momenta [13,15] can be excited and couple to Mie resonances to produce sharp Fano resonances. For a certain set of geometric parameters, these GSL modes undergo complete destructive interference, resulting in disappearance of the Fano features and formation of optical BICs. Full wave simulations and theoretical modeling using temporal coupled-mode theory (TCMT) formulated to include Lorenz-Mie scattering theory describe the origin of Fano resonances in different angular channels and the appearance of optical BICs. We discuss the geometric parameters for which a GSL satisfies the BIC condition and verify theoretical predictions with experimental measurements on single Si NW GSLs. This work realizes 1D BICs for the first time in the optical regime with true nanoscale lateral footprints, and we expect this result to inspire further research into the design of optical nanocavities.

As shown in Fig. 1(b), eigenmode analysis of NW GSL structures reveals GSL modes with quality factors (Q factors) that diverge to infinity within a range of p , indicating that these GSL modes are optical bound states with infinite lifetimes. The y component of the electromagnetic (EM) fields, H_y and E_y , of the two GSL eigenmodes are given in Figs. 1(c) and 1(d) (see the Supplemental Material [27] for full EM profiles). Each GSL mode is assigned with angular numbers of $m = 0$ or 1 based on the azimuthal order of field maxima. In Fig. 1(c),

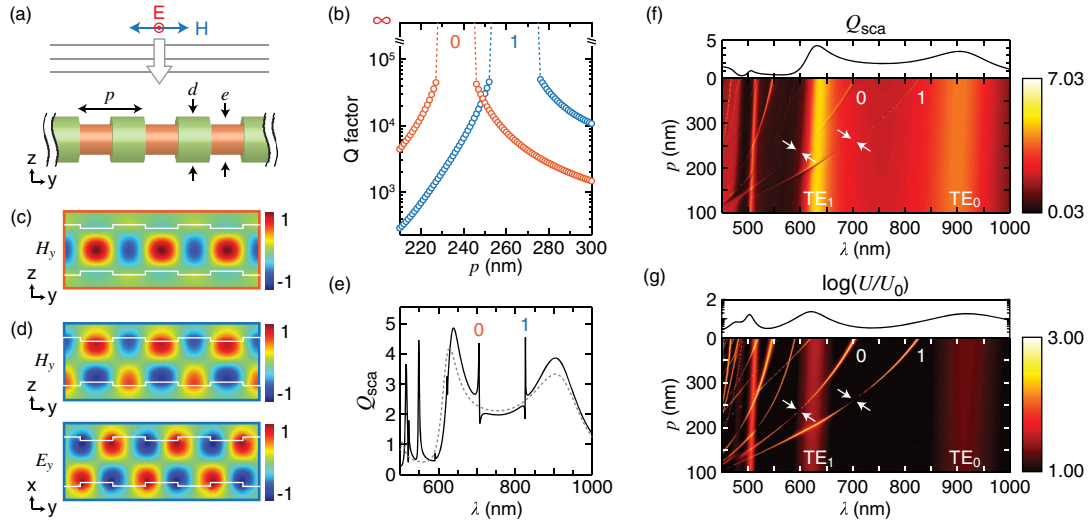


FIG. 1. Optical BICs in a NW GSL. (a) Geometry of a NW GSL under TE-polarized plane wave illumination, where the length of each segment is $p/2$. (b) Q factors of two GSL eigenmodes with varying p in a NW GSL with $d = 200$ nm, $e = 170$ nm. Modes are labeled with angular numbers $m = 0$ or $m = 1$. (c) H_y pattern of $m = 0$ GSL eigenmode. (d) H_y (upper) and E_y (lower) patterns of $m = 1$ GSL eigenmode. (e) Q_{sca} spectrum of a NW GSL with $d = 200$ nm, $e = 170$ nm, and $p = 400$ nm (solid black curve), and of a NW with $d = 185$ nm (gray dashed curve). (f),(g) Heat maps of (f) Q_{sca} and (g) $\log(U/U_0)$ for a NW GSL with varying p for fixed $d = 200$ nm and $e = 170$ nm. Single spectra for a uniform NW with $d = 185$ nm are presented on top of each heat map.

the $m = 0$ GSL mode has a definitive TE polarization (i.e., $E_y = 0$; not shown), and H_y exhibits an antiferromagnetic ordering of magnetic dipoles. In contrast, the $m = 1$ GSL mode in Fig. 1(d) is hybrid polarized, so both E_y and H_y are nonzero and must be considered.

Bulgakov and Sadreev [13,15] have categorized BICs arising in confined 1D geometries based on symmetry and propagation constant, and static BICs may have either even or odd symmetry under inversion. Odd modes are always symmetry protected from the free-space radiation, whereas even modes become decoupled from the radiation continuum only with certain geometric parameters. The $m = 0$ mode in Fig. 1(c) exhibits even symmetry and belongs to the latter case, and the BIC condition is achieved by tuning p as shown by the orange trace in Fig. 1(b). The $m = 1$ mode in Fig. 1(d), however, is odd in E_y but even in H_y . Thus, it is symmetry protected against the decay into the transverse-magnetic (TM) diffraction channel but reaches the bound state only when it also decouples from the TE continuum through the proper choice of p [Fig. 1(b), blue trace]. Previously, we reported a coupled excitation of guided modes in a NW GSL under excitation with a TM polarized plane wave [22], and although those modes have a similar symmetry to the $m = 1$ GSL mode in Fig. 1(d), Fig. 1(c) shows that the GSL modes are not limited to the guided modes and can possess different symmetry types.

A scattering efficiency (Q_{sca}) spectrum of a NW GSL with $p = 400$ nm is shown in Fig. 1(e) along with a reference Q_{sca} spectrum for a uniform NW. Because the value of p places the structure outside the range needed for a BIC, the Q_{sca} spectrum of the GSL exhibits two Fano

resonances resulting from coupling between the GSL mode and the background Mie resonance in the same angular channel. In the Q_{sca} heat map in Fig. 1(f), two sharp branches of GSL modes denoted with angular numbers $m = 0$ and 1 redshift with increasing p , while the background Mie resonances, denoted TE_0 and TE_1 , do not shift because of the fixed diameters. The $m = 0$ and 1 GSL branches show vanishing points at p values of 237 and 262 nm, respectively, where the modes become completely bound. These features are more clearly observed in the heat map of confined energy (U/U_0) in Fig. 1(g). While the p values producing a BIC, marked with arrows in Figs. 1(f) and 1(g), fall in the ranges of infinity Q factor for each mode in Fig. 1(b), the range of p satisfying the BIC condition is much narrower than the BIC ranges predicted by eigenmode calculations because of the directional illumination in plane wave simulations.

TCMT can be used to predict the optical coupling behavior in a NW GSL and has been used to interpret similar effects in photonic crystal slabs [26,28,29] and in spherical nanoparticles [30–33]. Here, we employ TCMT in the context of NWs by relating resonance parameters to the exact solutions of Mie coefficients [23]. For the scattering of a uniform, cylindrical NW, H_y under a TE plane wave ($H_x; H_z = 0$) is given by

$$H_y = \sum_{m=-\infty}^{\infty} [h_m^+ H_m^{(2)}(k\rho) + h_m^- H_m^{(1)}(k\rho)] e^{im\phi}, \quad (1)$$

where h_m^+ and h_m^- are amplitudes of the incoming and outgoing waves, $H_m^{(1)}$ and $H_m^{(2)}$ are the m th-order Hankel

functions, k is a wave vector, and ρ and φ are the polar coordinates [32]. We define a reflection coefficient by $R_m \equiv h_m^-/h_m^+$, and a single-mode TCMT expression is given by

$$\frac{d}{dt} A_m^{\text{Mie}} = (-i\omega_m^{\text{Mie}} - \gamma_m^{\text{Mie}}) A_m^{\text{Mie}} + \kappa_m^{\text{Mie}} h_m^+ \quad (2)$$

with $h_m^- = h_m^+ + d_m^{\text{Mie}} A_m^{\text{Mie}}$, where A_m^{Mie} , ω_m^{Mie} , and γ_m^{Mie} are the amplitude, eigenfrequency, and radiative decay rate of an m th-order Mie resonance, respectively, and κ_m^{Mie} and d_m^{Mie} are coupling coefficients to the incoming and outgoing plane waves, respectively. Absorptive loss is neglected for simplicity, and $\kappa_m^{\text{Mie}} = d_m^{\text{Mie}} = i\sqrt{2\gamma_m^{\text{Mie}}}$ by time-reversal symmetry [29]. The total Q_{sca} of a NW [32] is

$$Q_{\text{sca}} = \frac{2}{kr} \sum_{m=-\infty}^{\infty} \left| \frac{1 - R_m}{2} \right|^2, \quad (3)$$

where r is the NW radius. Noting the similarity of Eq. (3) to the Mie scattering formula, we can relate the scattering coefficient, $|(1 - R_m)/2|$ in Eq. (3), with an exact Mie scattering coefficient [23] to yield

$$\left| \frac{1 - R_m}{2} \right| = \left| \frac{\gamma_m^{\text{Mie}}}{i(\omega - \omega_m^{\text{Mie}}) + \gamma_m^{\text{Mie}}} \right| = |a_m|, \quad (4)$$

where a_m is an m th-order electric Mie coefficient responsible for scattering of a NW under TE polarization (analogously we can use the magnetic Mie coefficient, b_m , for TM polarization). Rearranging Eq. (4), as shown in the Supplemental Material [27], we get

$$\omega_m^{\text{Mie}} = \frac{2ia_m Q_m^{\text{Mie}} \omega}{(2iQ_m^{\text{Mie}} + 1)a_m \pm 1}, \quad (5)$$

where $Q_m^{\text{Mie}} = \omega_m^{\text{Mie}}/2\gamma_m^{\text{Mie}}$ is the Q factor of a Mie resonance on the order of 5 to 10 that can easily be estimated from numerical spectra. With ω_m^{Mie} and γ_m^{Mie} as functions of a_m , the modified TCMT can correctly produce the asymmetric line shapes of NW Mie resonances.

For a NW GSL, the full TCMT equation becomes

$$\begin{aligned} \frac{d}{dt} \begin{pmatrix} A_m^{\text{Mie}} \\ A_m^{\text{GSL}} \end{pmatrix} &= \left[-i \begin{pmatrix} \omega_m^{\text{Mie}} & \omega_m^c \\ \omega_m^c & \omega_m^{\text{GSL}} \end{pmatrix} - \begin{pmatrix} \gamma_m^{\text{Mie}} & 0 \\ 0 & \gamma_m^{\text{GSL}} \end{pmatrix} \right] \\ &\times \begin{pmatrix} A_m^{\text{Mie}} \\ A_m^{\text{GSL}} \end{pmatrix} + \begin{pmatrix} \kappa_m^{\text{Mie}} \\ \kappa_m^{\text{GSL}} \end{pmatrix} h_m^+, \end{aligned} \quad (6)$$

and $h_m^- = h_m^+ + d_m^{\text{Mie}} A_m^{\text{Mie}} + d_m^{\text{GSL}} A_m^{\text{GSL}}$, where A_m^{GSL} , ω_m^{GSL} , and γ_m^{GSL} are the amplitude, eigenfrequency, and radiative decay rate of an m th-order GSL mode, ω_m^c is the coupling strength between the Mie and GSL modes, and κ_m^{GSL} and

d_m^{GSL} are coupling coefficients of GSL modes to the incoming and outgoing plane waves, respectively.

We only consider the coupling of modes within the same angular channel [34], and using Eq. (6), we can fit the numerical Q_{sca} spectra to reproduce all scattering features. As an example, Figs. 2(a)–2(c) display Q_{sca} for $p = 220$, 260, and 320 nm at a fixed $d = 200$ nm and $e = 170$ nm, where total Q_{sca} obtained from TCMT (circles) are overlaid with numerical simulations (red curves). The case of

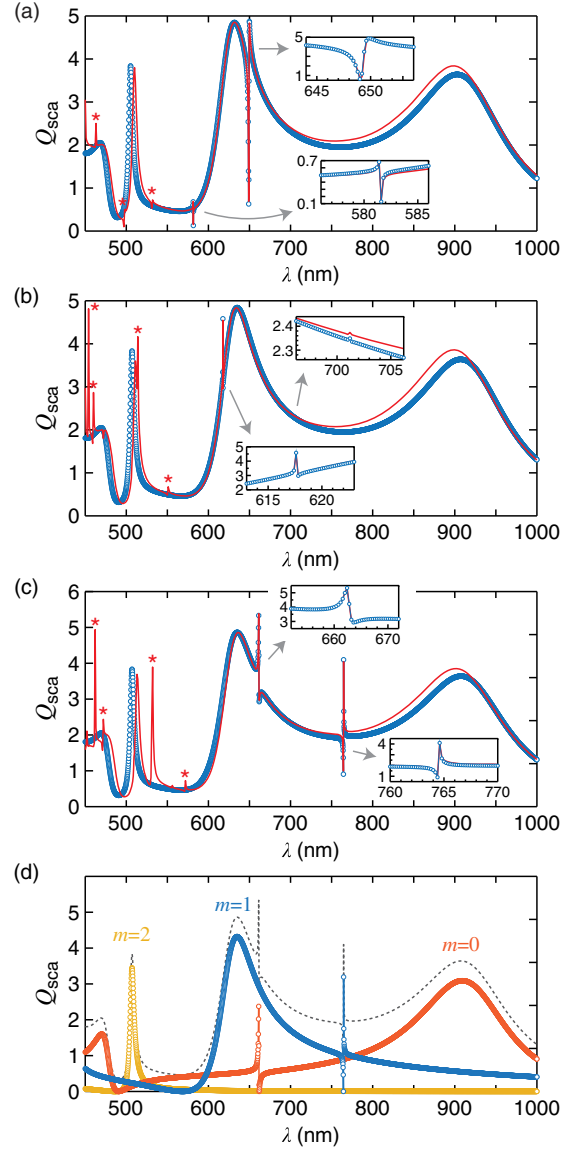


FIG. 2. Q_{sca} from TCMT and from full wave simulations. (a)–(c) Total Q_{sca} calculated by modified TCMT (blue circles) overlaid with numerical calculations (red curve) for a NW GSL with (a) $d = 200$ nm, $e = 170$ nm, and $p = 220$ nm; (b) $p = 260$ nm; or (c) $p = 320$ nm. Insets show magnified views near Fano resonances. Peaks marked with asterisks result from higher-order GSL modes not included in the TCMT. (d) Total Q_{sca} (dashed curve) from (c) decomposed into each angular channel (circles).

$p = 260$ nm satisfies the BIC condition, but shorter and longer p do not. Fano resonances appear for the shorter and longer p cases because the GSL modes couple with the Mie resonance ($\omega_m^c \neq 0$). At $p = 260$ nm, however, the $m = 1$ Fano peak almost completely vanishes at 701 nm [Fig. 2(b)]. The analytical Q_{sca} in Fig. 2(b) is obtained with both ω_1^c and $\gamma_1^{\text{GSL}} \approx 0$, implying the emergence of a perfectly bound optical state. Because the $m = 0$ GSL mode becomes bound at a slightly different p than $m = 1$ [cf. Figure 1(b)], it is still observed at ~ 618 nm but with a vanishing linewidth of ~ 0.2 nm. Figure 2(d) shows the total Q_{sca} (dashed curve) and separate Q_{sca} spectra from each angular channel calculated using Eq. (6) for the $p = 320$ nm NW GSL (circles). The two Fano resonances at ~ 661 and ~ 765 nm are separately observed in the $m = 0$ and 1 angular channels, respectively, and the long tails of the asymmetric Mie resonances permit Fano resonances to appear far away from the Mie maxima of the same channel.

The appearance of a BIC depends sensitively on illumination and structural geometry. For instance, BICs appear only at a Γ point because the symmetry of the BIC is distorted with a nonzero axial wave vector. As an example, Fig. 3(a) shows the Q factor of the $m = 1$ BIC mode of a NW GSL, calculated from the circled area in the inset band diagram, as a function of $kp/2\pi$ starting at Γ . The Q factor decreases from infinity as the wave vector deviates from Γ because the loss of illumination symmetry allows the mode to couple to the Mie resonance. Moreover, even at Γ , the range of p that produces a BIC (or an infinite Q factor) changes with different values of e at a fixed d , and there is a substantial widening of the p range producing a BIC as e approaches d , as shown in the eigenmode calculations in Fig. 3(b). When d and e are similar, the magnitude and mode volume of dipoles within each diameter segment are similar in magnitude (see Fig. S1 in the Supplemental Material [27]), so a broad set of p can produce the total destructive interference needed to form a BIC. However, as e deviates from d , the p range supporting a BIC narrows

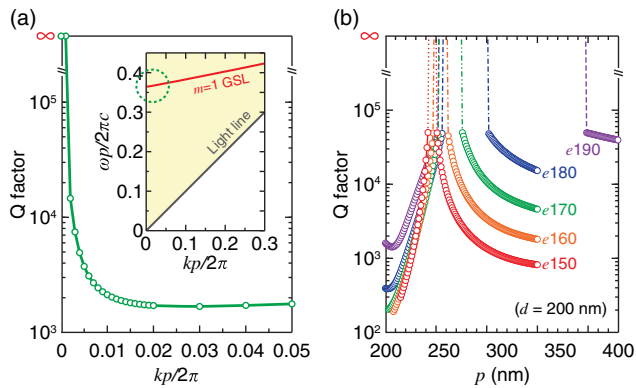


FIG. 3. Geometric dependence of Q factor. (a) Plot of Q factor as a function of $kp/2\pi$. (Inset) Band structure of the $m = 1$ mode. (b) Q factors of an $m = 1$ mode as a function of p with $d = 200$ nm and various e .

and eventually disappears (frequencies of BICs formed at different p and e are summarized in Fig. S2 in the Supplemental Material [27]).

We experimentally verified the scattering characteristics of NW GSLs fabricated by the encoded nanowire growth and appearance through vapor-liquid-solid growth and etching (ENGRAVE) technique [20,21]. A d close to 200 nm was chosen to allow direct comparison with the scattering heat map in Fig. 1(f), and p was varied from 200 to 400 nm with 50 nm increments to investigate the spectral shift and disappearance of the Fano resonances. To minimize variation in d and e , five 10 μm -long GSL sections with different p were encoded simultaneously in a single NW with 10 μm uniform segments separating each GSL, as shown by the scanning electron microscope (SEM) images in Fig. 4(a). Polarization-resolved transmissive single-NW extinction was measured in the visible range using a homebuilt laser microscope [22]. Simulated Q_{sca} corresponding to measured geometries and measured extinction spectra are shown in Figs. 4(b) and 4(c), respectively. Q_{sca} was simulated with a Gaussian beam (full width at half maximum of 1.5 μm) in the presence of material absorption to properly reflect the experiment.

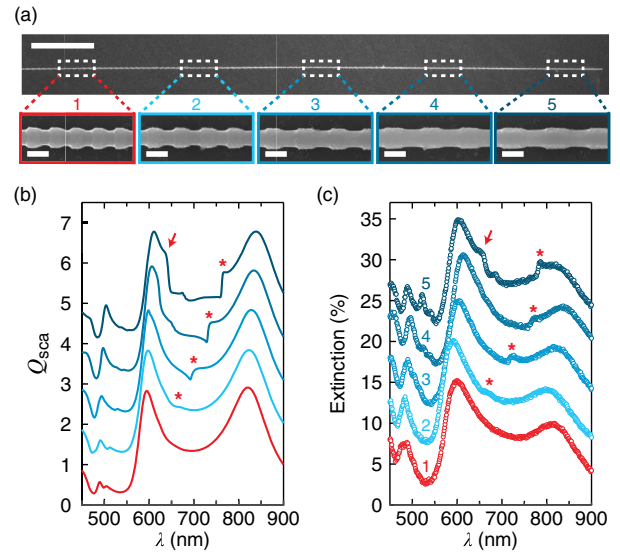


FIG. 4. Experimental extinction measurement of NW GSLs. (a) SEM image (upper panel) of a NW containing five GSL sections; scale bar, 10 μm . Magnified views (lower panels) of each GSL segment corresponding to the boxed regions in the upper panel; scale bars, 200 nm. Geometric parameters are $d = 189 \pm 2$ nm, $e = 141 \pm 2$ nm, $p = 201 \pm 4$ nm (GSL 1); $d = 185 \pm 1$ nm, $e = 135 \pm 2$ nm, $p = 250 \pm 4$ nm (GSL 2); $d = 186 \pm 1$ nm, $e = 147 \pm 2$ nm, $p = 300 \pm 3$ nm (GSL 3); $d = 185 \pm 1$ nm, $e = 153 \pm 2$ nm, $p = 348 \pm 4$ nm (GSL 4); and $d = 183 \pm 1$ nm, $e = 148 \pm 2$ nm, $p = 400 \pm 6$ nm (GSL 5). (b) Simulated Q_{sca} (spectra offset by 1) and (c) measured extinction (spectra offset by 5%) of GSLs. Red traces in both graphs represent spectra of a GSL at the BIC condition. Arrows and asterisks indicate the $m = 0$ and 1 Fano resonances, respectively.

For simulated spectra of a GSL with $p = 400$ nm [uppermost in Fig. 4(b)], two Fano resonances for $m = 0$ and $m = 1$ GSL modes are observed at ~ 645 and ~ 762 nm, as marked by the arrow and asterisk, respectively. Compared to the subnanometer linewidth shown in Fig. 1(e), a substantial broadening of the Fano line shape is observed because of absorptive loss and the finite beam [35]. An additional small peak at ~ 676 nm comes from the use of a finite beam [22]. As p decreases, the $m = 0$ peak gradually merges into the broad Mie resonance peak centered at ~ 600 nm, and the $m = 1$ peak (red asterisks) blueshifts and progressively decreases in magnitude. At $p = 230$ nm (red curve), the Fano peak vanishes because the mode becomes decoupled from the TE and TM radiation continua. The same pattern is observed in the experimentally measured extinction in Fig. 4(c). The extinction of GSL 5 (uppermost) shows the $m = 1$ Fano resonance at ~ 785 nm (red asterisk). The $m = 1$ Fano resonance blueshifts with decreasing p , and it eventually vanishes for GSL 1 (red circles), corresponding to the formation of a BIC. As a result, the extinction of GSL 1 looks identical to the typical extinction spectrum of a uniform NW, demonstrating the inaccessibility of the trapped modes by far-field illumination. Inclusion of absorption in eigenmode calculations shows a significant reduction of the Q factors to ~ 150 , and experimental Q factors, obtained from fitting the spectra, yield values of 95 to 180 that qualitatively agree with the calculations (see Fig. S3 in the Supplemental Material [27]).

In conclusion, we have demonstrated that NW GSLs support unique photonic modes that can be completely bound under a certain set of geometric parameters, and this Letter represents the first experimental demonstration of a BIC in a laterally confined 1D geometry in the optical regime. The bottom-up growth of Si NW GSLs through the ENGRAVE process offers several technological advantages, such as mechanical robustness from single-crystal materials, ability to electrogenerate photons inside the cavity through doping [36], and ease of device integration through templated growth [37]. Because the subwavelength lateral dimensions provide a true nanoscale footprint, these findings could enable the design of compact high- Q photonic devices such as single-NW photodetectors, lasers, sensors, and photonic circuits.

This research was primarily supported by the National Science Foundation (NSF; Grant No. DMR-1555001). S. K. acknowledges a Kwanjeong Scholarship, and J. F. C. acknowledges a Packard Fellowship for Science and Engineering. This work made use of instrumentation at the Chapel Hill Analytical and Nanofabrication Laboratory (CHANL), a member of the North Carolina Research Triangle Nanotechnology Network (RTNN), which is supported by the NSF (Grant No. ECCS-1542015) as part of the National Nanotechnology Coordinated Infrastructure (NNCI). We acknowledge the UNC Chapel Hill Research

Computing group for providing computational resources that contributed to these results.

*kyoungho@chungbuk.ac.kr

†jfcagoon@unc.edu

- [1] D. K. Gramotnev and S. I. Bozhevolnyi, *Nat. Photonics* **4**, 83 (2010).
- [2] A. F. Koenderink, A. Alu, and A. Polman, *Science* **348**, 516 (2015).
- [3] C. W. Hsu, B. Zhen, A. D. Stone, J. D. Joannopoulos, and M. Soljačić, *Nat. Rev. Mater.* **1**, 16048 (2016).
- [4] A. Kodigala, T. Lepetit, Q. Gu, B. Bahari, Y. Fainman, and B. Kante, *Nature (London)* **541**, 196 (2017).
- [5] S. T. Ha, Y. H. Fu, N. K. Emani, Z. Pan, R. M. Bakker, R. Paniagua-Dominguez, and A. I. Kuznetsov, *Nat. Nanotechnol.* **13**, 1042 (2018).
- [6] K. C. Y. Huang, M. K. Seo, T. Sarmiento, Y. J. Huo, J. S. Harris, and M. L. Brongersma, *Nat. Photonics* **8**, 244 (2014).
- [7] C. H. Cho, C. O. Aspetti, J. Park, and R. Agarwal, *Nat. Photonics* **7**, 285 (2013).
- [8] Z. F. Sadrieva and A. A. Bogdanov, *J. Phys. Conf. Ser.* **741**, 012122 (2016).
- [9] Y. Plotnik, O. Peleg, F. Dreisow, M. Heinrich, S. Nolte, A. Szameit, and M. Segev, *Phys. Rev. Lett.* **107**, 183901 (2011).
- [10] S. Weimann, Y. Xu, R. Keil, A. E. Miroshnichenko, A. Tünnermann, S. Nolte, A. A. Sukhorukov, A. Szameit, and Y. S. Kivshar, *Phys. Rev. Lett.* **111**, 240403 (2013).
- [11] C. W. Hsu, B. Zhen, J. Lee, S. L. Chua, S. G. Johnson, J. D. Joannopoulos, and M. Soljačić, *Nature (London)* **499**, 188 (2013).
- [12] J. Lee, B. Zhen, S. L. Chua, W. Qiu, J. D. Joannopoulos, M. Soljačić, and O. Shapira, *Phys. Rev. Lett.* **109**, 067401 (2012).
- [13] E. N. Bulgakov and A. F. Sadreev, *Phys. Rev. A* **92**, 023816 (2015).
- [14] E. N. Bulgakov and D. N. Maksimov, *Phys. Rev. Lett.* **118**, 267401 (2017).
- [15] E. N. Bulgakov and A. F. Sadreev, *Phys. Rev. A* **96**, 013841 (2017).
- [16] E. N. Bulgakov and A. F. Sadreev, *Phys. Rev. A* **97**, 063856 (2018).
- [17] M. V. Rybin, K. L. Koshelev, Z. F. Sadrieva, K. B. Samusev, A. A. Bogdanov, M. F. Limonov, and Y. S. Kivshar, *Phys. Rev. Lett.* **119**, 243901 (2017).
- [18] K. Koshelev, A. Bogdanov, and Y. Kivshar, *Sci. Bull.*, <https://doi.org/10.1016/j.scib.2018.12.003> (to be published).
- [19] M. A. Belyakov, M. A. Balezin, Z. F. Sadrieva, P. V. Kapitanova, E. A. Nenasheva, A. F. Sadreev, and A. A. Bogdanov, *arXiv:1806.01932*.
- [20] J. D. Christesen, C. W. Pinion, E. M. Grumstrup, J. M. Papanikolas, and J. F. Cahoon, *Nano Lett.* **13**, 6281 (2013).
- [21] J. D. Christesen, C. W. Pinion, D. J. Hill, S. Kim, and J. F. Cahoon, *J. Phys. Chem. Lett.* **7**, 685 (2016).
- [22] S. Kim, K. H. Kim, D. J. Hill, H. G. Park, and J. F. Cahoon, *Nat. Commun.* **9**, 2781 (2018).

- [23] C. F. Bohren and D. R. Huffman, *Absorption and Scattering of Light by Small Particles* (Wiley, New York, 1998).
- [24] G. Bronstrup, N. Jahr, C. Leiterer, A. Csaki, W. Fritzsche, and S. Christiansen, *ACS Nano* **4**, 7113 (2010).
- [25] L. Cao, P. Fan, E. S. Barnard, A. M. Brown, and M. L. Brongersma, *Nano Lett.* **10**, 2649 (2010).
- [26] S. H. Fan and J. D. Joannopoulos, *Phys. Rev. B* **65**, 235112 (2002).
- [27] See Supplemental Material at <http://link.aps.org/supplemental/10.1103/PhysRevLett.122.187402> for full EM profiles of GSL eigenmodes, detailed derivation of TCMT expressions, effects of e on BIC parameters with fixed d , experimental Q factors, and details of the experiments and simulations.
- [28] S. Fan, W. Suh, and J. D. Joannopoulos, *J. Opt. Soc. Am. A* **20**, 569 (2003).
- [29] S. Wonjoo, W. Zheng, and F. Shanhui, *IEEE J. Quantum Electron.* **40**, 1511 (2004).
- [30] R. E. Hamam, A. Karalis, J. D. Joannopoulos, and M. Soljacic, *Phys. Rev. A* **75**, 053801 (2007).
- [31] Z. C. Ruan and S. H. Fan, *J. Phys. Chem. C* **114**, 7324 (2010).
- [32] Z. Ruan and S. Fan, *Phys. Rev. Lett.* **105**, 013901 (2010).
- [33] C. W. Hsu, B. G. DeLacy, S. G. Johnson, J. D. Joannopoulos, and M. Soljacic, *Nano Lett.* **14**, 2783 (2014).
- [34] P. Fan, Z. Yu, S. Fan, and M. L. Brongersma, *Nat. Mater.* **13**, 471 (2014).
- [35] Z. F. Sadrieva, I. S. Sinev, K. L. Koshelev, A. Samusev, I. V. Iorsh, O. Takayama, R. Malureanu, A. A. Bogdanov, and A. V. Lavrinenko, *ACS Photonics* **4**, 723 (2017).
- [36] D. J. Hill, T. S. Teitsworth, S. Kim, J. D. Christesen, and J. F. Cahoon, *ACS Appl. Mater. Interfaces* **9**, 37105 (2017).
- [37] M. Knoedler, N. Bologna, H. Schmid, M. Borg, K. E. Moselund, S. Wirths, M. D. Rossell, and H. Riel, *Cryst. Growth Des.* **17**, 6297 (2017).